Local-spin-selective x-ray absorption and x-ray magnetic circular dichroism of MnP

F.M.F. de Groot, S. Pizzini, and A. Fontaine
Laboratoire pour l'Utilisation du Rayonnement Electromagnétique, Université Paris-Sud, Bâtiment 209D, 91405 Orsay, France

K. Hämäläinen
Department of Physics, P.O. Box 9, Helsinki FIN-00014, University of Helsinki, Finland

C.C. Kao and J.B. Hastings
National Synchrotron Light Source, Brookhaven National Laboratory, Upton, New York 11973
(Received 5 July 1994; revised manuscript received 22 September 1994)

The local-spin-selective x-ray-absorption spectrum and the magnetic-circular-dichroism spectrum are measured at the manganese K edge of MnP. Both spectra show the presence of a strong spin polarization at the edge. A comparison of the two techniques makes it possible to determine the energy dependence of the Fano factor. It is found that the Fano factor is -4% at the edge but it decreases quickly over an energy range of 10 eV to values lower than 1%. The local-spin-selective x-ray-absorption spectrum is compared to the empty density of states as determined from a local-spin-density band-structure calculation. The use of the $K\beta$ detection yields a spectrum with considerably better resolution, which offers new possibilities for more detailed comparisons with electronic-structure models.

I. INTRODUCTION

In this paper we compare two recent techniques to study the magnetic structure of solids: local-spin-selective x-ray absorption and x-ray magnetic circular dichroism (MCD).

Local-spin-selective x-ray absorption was exploited by Hämäläinen and co-workers.[1] In this technique the K-edge x-ray-absorption spectrum is measured by detecting the $K\beta$ x-ray-emission ($3p \rightarrow 1s$) decay channel at two different energy positions. One can separate the $K\beta$ x-ray-emission spectrum into an internally referenced spin-up part and a spin-down part[2] and by selecting these parts of the spectrum one is able to obtain a local-spin selectivity in the K-edge absorption spectrum. This technique bears resemblance to "spin-polarized" photoelectron diffraction (PED),[3] which also uses the $3p$ core spectrum for the spin selection. The use of a core spectrum for the spin selectivity implies that the spin is referenced to the local situation in the solid. For a ferromagnet this is equivalent to an external referenced technique, like x-ray MCD, as all sites bear a magnetic moment in the same direction. For an antiferromagnetic sample the sites are 50% spin up and 50% spin down and their, eventual, dichroism effect is canceled. However, in case one uses an electron created from a core state this observes the situation referenced to the spin direction of its site. Looking from the outside of the system, as one would do with a Mott detector, the electrons from these two sites are antiparallel. But both are parallel with respect to their local valence electron spin density; hence they appear at equal energy in the $3p$ photoemission or $K\beta$ x-ray-emission spectrum and at a different energy than the electrons which are antiparallel to the local spin direction. Therefore by selecting the energy of the $K\beta$ spectrum one measures the local difference in spin direction for antiferromagnets as well as ferromagnets.

X-ray-absorption spectra at K edges are described with single-particle models.[4] The process is described as the excitation of the $1s$ core electron to an empty state of p symmetry with respect to the site of excitation. The absorption cross section (μ) is given as the density of empty states (ρ) multiplied by the (squared) dipole matrix element coupling the $1s$ core wave function with the p wave functions (R^2).[5] In case of local-spin-selective x-ray absorption one measures the cross section independently for spin up and spin down, hence as a function of the excitation energy (ω):

$$\mu_\uparrow(\omega) - \mu_\downarrow(\omega) = [R^2_\uparrow(\omega)\rho_\uparrow(\omega)] - [R^2_\downarrow(\omega)\rho_\downarrow(\omega)] \ . \quad (1)$$

Note that experimentally it is not possible to distinguish matrix element effects from density of states. This distinction is made only because they are separated in the theoretical analysis.

With MCD one probes the same x-ray-absorption spectrum with circularly polarized x rays. X-ray MCD effects have been observed by Schütz and co-workers.[6] The difference between left (μ_L) and right (μ_R) circular x rays is proportional to the difference in the spin polarization of the empty states multiplied by their matrix element. The proportionality factor is the so-called Fano factor (P):[7]

$$\mu_L - \mu_R = P([R^2_\uparrow\rho_\uparrow] - [R^2_\downarrow\rho_\downarrow]) \ . \quad (2)$$

The energy dependence has been omitted in Eq. (2). In principle the density of states, matrix elements, and Fano factor all can be energy dependent. The Fano factor originates from the fact that for K edges the MCD

is caused by the spin-orbit coupling of the final states. With circularly polarized x rays one excites to p states with either $j = 3/2$ or $j = 1/2$. Without spin-orbit coupling in these p states there is no dichroic effect visible. Because of the spin-orbit coupling the radial matrix elements for $p_{3/2}$ and $p_{1/2}$ are not exactly equal. Spin-orbit coupling draws in the nodes of the $j = 1/2$ wave function and pushes out those of $j = 3/2$. Because of normalization, the net difference between the two wave functions is particularly large in the core region where overlap with the $1s$ wave function takes place. It is this mechanism which leads to a difference of the $R_{3/2}$ or $R_{1/2}$ matrix elements and hence to the Fano factor. This spin-orbit effect can be separated from the effects due to the spin polarization of the radial matrix elements and the (experimentally inseparable) spin polarization of the density of states. From the paper of Fano one finds:[7]

$$P = \frac{1+2X}{2+X^2} \text{ with } X = \frac{2R_{3/2}+R_{1/2}}{R_{3/2}-R_{1/2}} . \quad (3)$$

For small (< 10%) differences between the matrix elements this equation simplifies to

$$P \approx \frac{8}{3}\frac{(R_{3/2}-R_{1/2})}{(R_{3/2}+R_{1/2})} . \quad (4)$$

The Fano factor is directly proportional to the difference in the radial matrix elements of the two spin-orbit split states. In the analysis of x-ray MCD it is often assumed that both the Fano factor and matrix elements are energy independent and also that the matrix elements are equal for spin-up and spin-down electrons. With these assumptions one can eliminate the matrix elements from the formula by dividing the difference spectrum by the sum spectrum and one obtains the familiar formulation of x-ray MCD,[6]

$$\frac{\mu_L(\omega)-\mu_R(\omega)}{\mu_L(\omega)+\mu_R(\omega)} = P \cdot \frac{\rho_\uparrow(\omega)-\rho_\downarrow(\omega)}{\rho_\uparrow(\omega)+\rho_\downarrow(\omega)} . \quad (5)$$

However, the approximations made to obtain Eq. (5) are not clearly established: The Fano factor is not guaranteed to be energy independent and for example the original paper of Fano[7] indicates a strong energy dependence. Also the radial matrix elements for spin up and spin down are not necessarily equal.[8]

In fact the comparison of local-spin-selective x-ray absorption and x-ray MCD can shed some light on this matter. By comparing Eqs. (1) and (2) one notices that local-spin-selective and x-ray MCD both give a measure of the spin polarization of the empty states (both multiplied with matrix elements). By dividing Eqs. (1) and (2) one directly determines the Fano factor, including its eventual energy dependence:

$$\frac{\mu_L(\omega)-\mu_R(\omega)}{\mu_\uparrow(\omega)-\mu_\downarrow(\omega)} = P(\omega) . \quad (6)$$

The determination of the energy dependence of the Fano factor, by dividing the x-ray MCD and local-spin-selective x-ray-absorption experiments, is discussed in Sec. III E.

A. Determination of the x-ray-absorption cross section

The transmission detected x-ray-absorption cross section ($I^T_{\rm XAS}$) is given as

$$I^T_{\rm XAS}(\omega) = [L_{1s}G_E]R^2(\omega)\rho(\omega) . \quad (7)$$

All broadening factors are placed in square brackets: The $1s$ core state has a finite lifetime which gives rise to a Lorentzian broadening (L_{1s}). The width of the lifetime broadening is indicated with Γ_{1s}. Furthermore, the incoming x ray has a spread in energy which is approximated as a Gaussian broadening of the x-ray-absorption cross section (G_E).

The combination of an x-ray-absorption and x-ray-emission process is named both resonant x-ray emission[9] as well as inelastic x-ray scattering.[10] The complete formulation of this combined process has been given in Ref. 10. By omitting the spatial (angular) degrees of freedom one obtains

$$I(\omega,\omega') = [L_{3p}(\omega,\omega')G_E] \times \sum_{3p}\left|\sum_{1s}\frac{\langle 3p \mid r_q \mid 1s\rangle\langle 1s \mid r_q \mid \varepsilon\rangle}{\omega - E_{1s} - i\Gamma_{1s}}\right|^2 . \quad (8)$$

ω' indicates the decay energy, ω the excitation energy. The experimental broadening (G_E) includes both the energy spread of the incoming x ray and the resolution of the detector. From this general formulation one can derive the equations for the x-ray-absorption cross section measured at a particular decay energy [$I^{\omega'}_{\rm XAS}(\omega)$] and the x-ray-emission cross section at a particular excitation energy [$I^{\omega}_{\rm XES}(\omega')$]. For $1s$ intermediate states interference effects do not occur and one can abandon the denominator. Because of the coherence of excitation and decay processes the lifetime broadening of the intermediate state disappears from the formula and one obtains

$$I^{\omega'}_{\rm XAS}(\omega) = C_{\omega'}[L_{3p}G_E]R^2(\omega)\rho(\omega) . \quad (9)$$

The broadening factors are given in square brackets. The proportionality factor ($C_{\omega'}$) is the $K\beta$ ($3p \rightarrow 1s$) x-ray-emission decay strength at the detector energy ω'.

Similarly one can obtain the $K\beta$ x-ray-emission cross section at a particular excitation energy:

$$I^{\omega}_{\rm XES} = C_\omega[L_{1s}L_{3p}G_E]\sum_{3p} \mid \langle 3p \mid r_q \mid 1s\rangle \mid^2 . \quad (10)$$

The proportionality factor C_ω is given by the density of states to which the $1s$ electron is excited ($R^2\rho$). Notice that for the decay process the broadening factors include the $1s$ lifetime.

The rest of the paper is organized as follows: Section II discusses the experimental aspects of both local-spin-selective x-ray absorption and x-ray MCD. In Sec. III A we discuss the interpretation of the $K\beta$ x-ray-emission spectrum and in Sec. III B the data treatment of the resulting local-spin-selective x-ray-absorption spectrum.

The results are compared with those obtained by x-ray MCD in Sec. III C and the local-spin-selective x-ray-absorption spectrum is compared with the empty density of states as obtained from a local-spin-density (LSD) band-structure calculation in Sec. III D. Finally Sec. III E discusses the determination of the Fano factor.

II. EXPERIMENT

The local-spin-selective x-ray-absorption experiment was carried out on the X25 hybrid wiggler beam line[11] at the National Synchrotron Light Source at Brookhaven National Laboratory. A double-crystal Si(220) monochromator which produces an incident x ray with an intensity of 10^{11} photons/sec and a resolution of 0.7 eV [full width at half maximum (FWHM)] was used. The $K\beta$ x-ray emission was analyzed with a Rowland circle spectrometer equipped with a spherically bent Si(440) crystal and a NaI scintillation counter.[12,13] At 6.5 keV the analyzer resolution was 0.3 eV. The average count rate at the fluorescence peak above the absorption edge was 1500 counts per second with a measured background of less than one count per second. The total beam time for the experiment was 5 days.

The x-ray MCD experiment was performed at the energy-dispersive x-ray-absorption beam line of the DCI storage ring at the Laboratoire pour l'Utilisation du Rayonnement Electromagnetique (LURE). Right circularly polarized x rays with a degree of polarization of 80% were selected by positioning a 1 mm vertical slit at 3 mrad below the synchrotron orbit plane. The curved Si(111) dispersive monochromator[14] focuses at the sample site with a resolution of 1.2 eV (FWHM). The whole spectrum is measured at once with a photodiode array detector made of 1024 pixels.[15] The advantages of the dispersive geometry, i.e., stability and high throughput, are discussed in detail in Ref. 15. A magnetic field of 1.0 T was applied by an electromagnet and the field direction was alternated to obtain field directions parallel and antiparallel to the propagation direction of the x-ray beam. The magnetic field was flipped each minute with a dead time of 8 sec. The total measurement time was 16 h.

For the x-ray MCD measurements a single-crystal MnP sample which was grounded and dissolved in cyclohexane was used. The solution was poured onto a 10 μm micropore filter. In this manner a thin layer of uniform thickness is achieved. The layer is covered with collodion for protection. The $K\beta$ fluorescence measurements were carried out on a single crystal of MnP. MnP has a Curie point (T_C) at 291 K and below 46 K the ferromagnetic ordering changes to a fanlike ordering. The magnetic phase diagram has been given by Komatsubara and co-workers.[16] Experiments were carried out in both the ferromagnetic phase (at 150 K) and the paramagnetic phase (at 350 K).

III. RESULTS AND INTERPRETATION

A. $K\beta$ x-ray-emission spectrum

In local-spin-selective x-ray absorption the detection system for the absorption spectrum is a fluorescence detector which is tuned to the energy of the $K\beta$ x-ray-emission spectrum. Before using this decay channel as a detector we first study its shape and its variation with excitation energy. The questions we have to answer are (1) does the $K\beta$ decay channel result in a constant proportionality factor, and (2) what is the spin polarization at different points in the spectrum; hence what are the best energy points to choose for the detector.

Figure 1 shows in one plot both the K-edge x-ray-absorption and the $K\beta$ x-ray-emission spectra of MnP. The x-ray-absorption edge is positioned at 6538 eV and the peak maximum of the $K\beta$ ($3p \rightarrow 1s$) decay is positioned at about 6490 eV. The energy difference of approximately 48 eV identifies with the binding energy of a $3p$ electron.

The shape of the $K\beta$ x-ray-emission spectra is largely determined by final state effects. The final state of the $K\beta$ x-ray-emission process contains a $3p$ hole, which is known to interact strongly with the partly filled $3d$ valence band. This $3p3d$ interaction gives rise to so-called multiplet effects which can be studied within the framework of crystal field theory,[2] or in case of strong influences from covalency with an Anderson impurity Hamiltonian.[17] The $K\beta$ spectrum of MnP shows close correspondance to the crystal field multiplet calculations for Mn^{3+} ions as given by Peng and co-workers.[2] The degree of spin polarization can be estimated to be more than 90% spin down for the main peak, while at energies more than 10 eV from the peak position the spectrum is 100% spin up apart from the Lorentzian tail of the main peak.

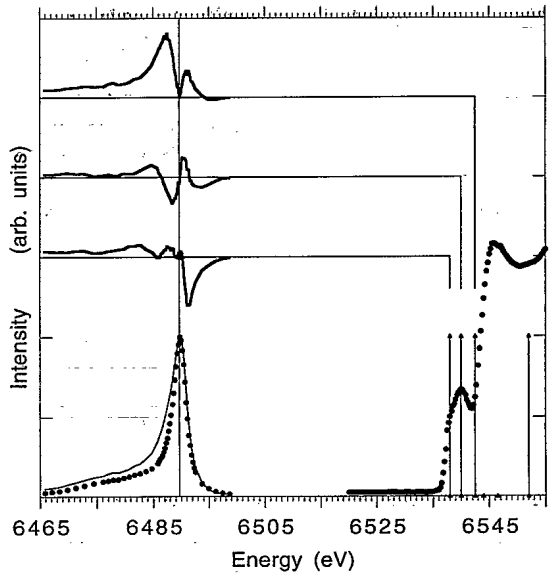

FIG. 1. $K\beta$ x-ray-emission (left) and K-edge x-ray-absorption spectrum (right) of MnP. The $K\beta$ spectra are normalized to 1 (see text). They given for the excitation energies 6552 eV (dots) and 6542 eV (thin line). At the upper left difference spectra with the 6552 eV spectrum are given for the excitation energies 6538 eV, 6540 eV (middle) and 6542.5 eV (top). These excitation energies are indicated with solid triangles in the x-ray-absorption spectrum and with the extension of the base line for the difference spectra.

The spin-down spectrum can best be measured at the peak position of the $K\beta$ decay (6489.7 eV). For the measurement of the spin-up spectrum we chose a distance of 17 eV to the main peak. The spectrum shows a long tail where the intensity does not decrease quickly and to limit the effects of the Lorentzian tail the energy difference to the main peak is chosen as large as possible.

The shape of the $K\beta$ spectrum has also consequences for the effective broadening of the local-spin-selective x-ray-absorption spectra. This broadening is given by Eq. (9) and one expects a considerable increase in the resolution because the $1s$ lifetime broadening disappears. This reasoning is indeed correct for the main peak which is essentially a single peak broadened according to Eq. (10). However, at the tail position the $K\beta$ spectrum is essentially flat; in other words within the $K\beta$ spectrum the summation over $3p$ states in Eq. (10) shows a range of states that can be detected. Because the broadening of the $K\beta$ spectrum includes Γ_{1s} one can detect all $3p$ states within this energy spread. This implies for the x-ray-absorption spectrum that the proportionality factor (with its summation over $3p$ states) contains the $1s$ lifetime broadening, which yields a total broadening of $\Gamma_{1s} \times \Gamma_{3p}$. Thus the effective broadening obtained by putting the detector at the $K\beta$ spectrum can vary between Γ_{3p} for a single $3p$ final state (sharp peak) and $\Gamma_{1s} \times \Gamma_{3p}$ for a flat region of the spectrum.

To determine the variation in the $K\beta$ x-ray-emission spectrum we have measured a series of six spectra taken at excitation energies as indicated with solid triangles on the base line at the absorption edge (Fig. 1, right side). On the left side of Fig. 1 we show the $K\beta$ x-ray-emission spectra taken at 6542.5 eV excitation energy (solid line) and at 6552 eV (dots), both normalized to 1. The relative strengths of the $K\beta$ x-ray-emission spectra are given by the density of states at the respective excitation energies [cf. Eq. (9)]. For the figure we have normalized all spectra to one in order to make their shape differences better visible. For example, if a spectrum is broader, the difference of the spectra shows two positive peaks at both sides of the maximum, etc. The 6552 eV spectrum can be considered the nonresonant $K\beta$ x-ray-emission spectrum. We plot the difference spectra with this nonresonant spectrum for 6542.5 eV (upper left, top), 6540 eV (middle), and 6538 eV (down). The energies are indicated in the figure by the extension of the zero line to the excitation spectrum on the right. The difference spectra show that there is a considerable variation in the spectral shapes.

We analyze these variations in the normalized $K\beta$ spectra using Eq. (10). The 6538 eV spectrum (bottom) has lower intensity on the high energy side. This is caused by the resonant Raman effect.[18,19] If the excitation energy (ω) is smaller than the edge energy ($\Omega \approx 6538$ eV) plus the lifetime broadening ($\Gamma \approx 1.5$ eV), one does not reach the full $K\beta$ x-ray-emission intensity. A quantative analysis of the transition from the resonant Raman regime ($\omega < \Omega - \Gamma$), via the intermediate regime, to the normal fluorescence regime ($\omega > \Omega + \Gamma$) is given by Hämäläinen and co-workers.[19]

The 6542.5 eV spectrum is broader; hence its difference spectrum (top) has higher intensity on both sides of the peak position. This broadening effect is caused by the shape of the density of states ($R^2\rho$) at the particular excitation energies. A flat density of states [Eq. (10), C_ω = const.] results in the broadening $[L_{1s}L_{3p}G_E]$. A mimimum in the density of states, as for 6542.5 eV, will make the spectrum broader because C_ω increases at the positions of the lobes of the broadening. Likewise a maximum in the density of states, as for 6540 eV, makes the spectrum appear sharper. Thus the density of states and for $\omega < \Omega + \Gamma$ also the resonant Raman effect modify the shape of the $K\beta$ x-ray-emission spectrum. It is important to note that the $3p \rightarrow 1s$ matrix elements are not affected. This implies that the proportionality factor for the use of the decay channel for x-ray absorption in Eq. (9) is indeed a constant.

B. Local-spin-selective x-ray-absorption spectra

The consequences for local-spin-selective x-ray absorption are the following: (a) The $K\beta$ x-ray-emission cross section gives rise to a constant proportionality factor. (b) The peak spectrum taken at 6489.7 eV relates to more than 90% spin down and has approximately a broadening $[L_{3p}G_E]$; the tail spectrum taken at 6472.7 eV relates to 100% spin up and has a broadening which can be approximated as $[L_{1s}L_{3p}G_E]$. (c) The Lorentzian tail of the main peak will appear in the spectrum taken at 6472.7 eV, the so-called resonant Raman effect.[19]

The bottom of Fig. 2 shows the normalized local-spin-selective x-ray-absorption spectra: the spin-down spectrum taken 6489.7 eV (solid line) and the spin-up spec-

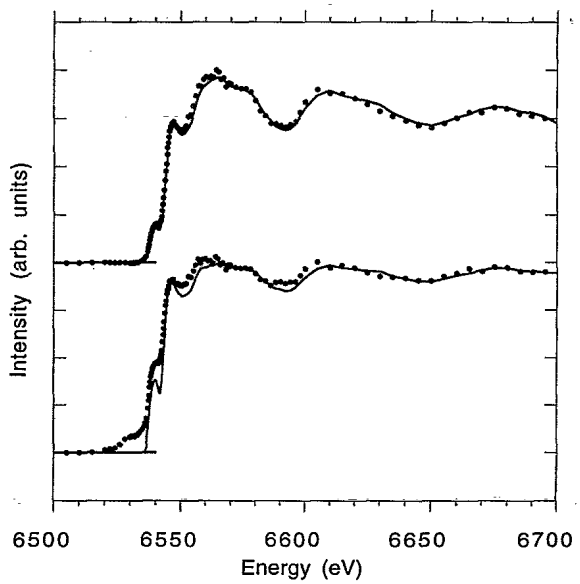

FIG. 2. Bottom: the raw x-ray-absorption spectra taken at 6489.7 eV (spin down, solid line) and 6472.7 eV (spin up, dots). Top: the spin-down (solid line) and spin-up (dots) local-spin-selective x-ray-absorption spectra after data processing. The spectra are normalized to each other by integration of the total spectrum.

trum taken at 6472.7 eV (dots).

In order to determine their difference one has to take care that the effects which affect the spectral shapes are made equal for spin up and spin down. The proportionality factor (a) can be taken care of by normalizing both spectra over the full energy range of 200 eV. The resonant Raman effect (c) is clearly visible as the onset of the spin-up spectrum at 17 eV lower energy than the spin-down spectrum. The intensity of the resonant Raman effect at 17 eV is less than 1% but because the intensity of the tail is small compared to the main peak the resonant Raman effect is clearly visible. One can correct the spin-up spectrum for the resonant Raman effect essentially by subtracting the broadened spin-down spectrum shifted over 17 eV. The spin-up spectrum (dots) at the top shows the resonant-Raman-corrected spectrum. The spin-down spectrum is very sharp which makes a comparison to electronic structure models more precise (see next section). However, to make possible a comparison with the spin-up spectrum the broadening of the spin-down spectrum must be adapted. If the spin-up spectrum is broadened with $[L_{1s}L_{3p}G_E]$ and the spin-down spectrum with $[L_{3p}G_E]$, the spin-down spectrum has to be given an extra broadening with the $1s$ lifetime broadening. Because the experimental broadenings are not exactly known we have optimized this additional Lorentzian broadening in order to make the total broadening of both spectra equivalent. We determined a value of 1.5 eV (FWHM). Both processed spectra, also corrected for the absorption cross section, are shown at the top. The final difference obtained is very small. In the next sections we will discuss the region at the edge in more detail.

The local-spin-selective x-ray absorption has been measured in the ferromagnetic phase at 150 K and in the paramagnetic phase at 350 K. Within the sensitivity obtained no differences are observable between the data taken at 350 K and 150 K. This implies that also above the Curie temperature there is a local moment which interacts with the $3p$ core hole. Though not ordered this local moment still offers a possibility to distinguish between local spin-up and spin-down states using the $K\beta$ channel.

C. Comparison with x-ray MCD

Figure 3 shows the comparison between the local-spin-selective x-ray-absorption spectrum and the x-ray MCD spectrum in the energy range from 6530 to 6570 eV. The two local-spin-selective x-ray-absorption spectra are given at the bottom for spin up (solid line) and spin down (dashed line). Their difference is indicated in the top spectrum with the open circles. If one normalizes the absorption spectra to 1.0, the difference reaches a maximum of +4% at 6543.5 eV indicated with a vertical line. In the difference spectrum a shoulder is visible at 6538.5 eV also indicated with a vertical line. The middle spectrum shows the x-ray-absorption spectrum measured in transmission with right circular polarized x rays. The spectrum measured with the opposite magnetization direction is not visibly different. The x-ray MCD effect, indicated at the top with the solid dots, has a maximum difference of −0.08%. The transmission x-ray-absorption spectral shape is similar to the local-spin-selective x-ray-absorption spectra at the bottom. A difference is that the experimental broadening is larger for the x-ray MCD experiment. It can be seen that both the local-spin-selective x-ray-absorption spectrum and the x-ray MCD spectrum show relatively large effects between 6535 and 6545 eV. While for x-ray MCD the effect diminishes at higher energy for local-spin-selective x-ray-absorption the difference spectrum is of the same order of magnitude. In Sec. III E we compare both spectra quantitatively to determine the energy dependence of the Fano factor.

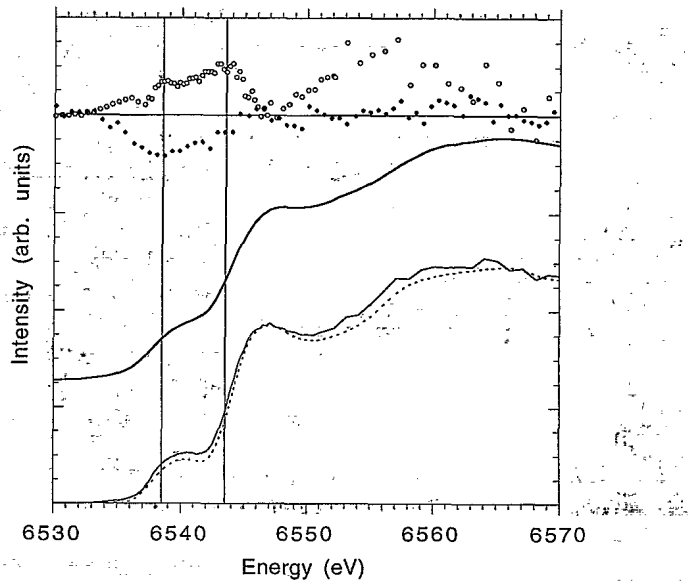

FIG. 3. Bottom: the local-spin-selective x-ray-absorption spectra for spin up (solid line) and spin down (dashed line). Middle: the x-ray-absorption specrum taken with transmission. Top: comparison of the local-spin-selective x-ray-absorption difference spectrum (open circles) and the x-ray MCD spectrum (solid points, multiplied by 50). The two vertical lines indicate the peak maximum for the difference spectrum and a shoulder at lower energy corresponding with the minimum for the x-ray MCD.

D. Comparison with spin-polarized density of states

Following Eq. (1) the spin-polarized x-ray-absorption spectra correspond to the spin polarization of the empty states of manganese p character. Qualitatively the electronic structure of MnP can be described as a $3d$ band crossing the Fermi level. In turn this spin-polarized band affects the spin polarization of the manganese p-DOS. To make a quantitative comparison, the empty density of states of MnP are calculated using local spin density (LSD) band-structure calculations.

The calculation has been carried out with the linear muffin-tin orbital (LMTO) method[20] using the atomic

sphere approximation (ASA).[21] MnP is calculated in its P_{nma} crystal structure with per unit cell four manganese ions and four phosphor ions. Both ions are positioned in the Wyckoff 4*c* position of the space group with the parameters $x = 0.005, z = 0.20$, for Mn and $x = 0.19, z = 0.57$ for P.[22] The radii of Mn and P are chosen equal at 2.7075 au. For the self-consistent LMTO-ASA calculation 4*s*, 4*p*, and 3*d* orbitals are included for Mn and 4*s* (downfolded[21]), 3*p* and 3*d* orbitals for P. The 4*f* functions are only used in the expansions.[21] The calculations are carried out with $8 \times 12 \times 8 = 768$ k points in the Brilloin zone which relates to 175 irreducible k points. Details concerning the calculations will be discussed in Ref. 23 for a series of comparisons to x-ray absorption spectra.

Figure 4 compares the local-spin-selective x-ray-absorption spectra (μ) with the broadened manganese spin-polarized *p*-projected density of states (ρ_p). At the top the local-spin-selective x-ray-absorption spectra are given for spin up (solid line) and spin down (dashed line). In the middle the ρ_p curves are given for spin-up (solid line) and spin-down (dashed line). The broadenings used are the experimental broadening and the 1*s* lifetime broadening. ρ_p is given only up to 22 eV above the Fermi level because at higher energies the errors become too large due to the limited basis set used. The density of states is aligned to the x-ray-absorption spectra at the position of the first peak in the spin-difference spectrum. The vertical line indicates the position of the Fermi level in the calculation. A similarity can be observed between μ and ρ_p, both in the general shape as in the exchange splitting between spin up and spin down.

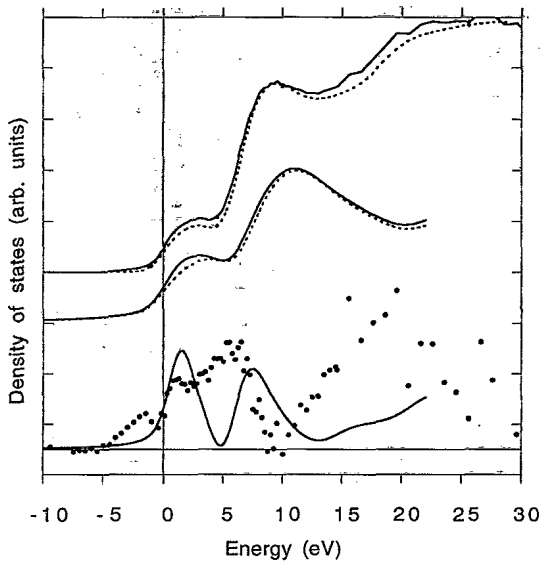

FIG. 4. Top: the local-spin-selective x-ray-absorption spectra for spin up (solid line) and spin down (dashed line). Middle: the broadened manganese *p*-projected density of states of MnP for spin up (solid line) and spin down (dashed line), aligned with its Fermi energy at the position of the edge (see text). Bottom: the local-spin-selective x-ray-absorption *difference* spectrum (dots) compared to the spin difference of the densities of states (solid line).

At the bottom of Fig. 4 the spin difference of the x-ray-absorption spectra (dots) is compared with the spin difference in ρ_p. Both are multiplied by 10 comparing to the scale of the absorption spectra in the figure. Notice that in the experimental difference spectrum a structure is visible below the Fermi level. This structure is also visible in the spin-up spectrum at the top (solid line), which does not approach zero as expected at the edge. This is an artifact of the data treatment due to the small errors induced by the resonant Raman subtraction procedure.

The band-structure calculation yields two broad bands: Between −7 eV and +5.5 eV (referred to the Fermi level), the band is formed by the strongly covalent interaction of the manganese 3*d* states with the 3*p* (+*s*) states from phosphor. We will name it the 3*d* band. From about 6.5 eV to higher energy a new structure occurs which is dominantly formed by the antibonding phosphor 3*p* states.[23] From 5.5 eV to 6.5 eV a gap exists. The two peaks visible in the broadened ρ_p spectra relate to respectively the Mn 3*d* band and the antibonding P 3*p* band. These two peaks are also visible in the x-ray-absorption cross section. A difference is that in μ the maximum of the second peak is shifted to lower energy, both for spin up and spin down. For the spin difference one observes two positive structures in both μ and ρ_p. The positive sign indicates that the spin-up density of states is shifted to lower energy compared to the spin-down density of states. The fact that the spin difference is of equal magnitude (+4% maximally in the first two peaks) in μ and ρ_p indicates that the matrix elements for spin up and spin down are approximately equal [cf. Eq. (1)]. A difference between $\mu^+ - \mu^-$ and $\rho_p^+ - \rho_p^-$ is that in $\mu^+ - \mu^-$ the dip between the two peaks has filled up. This is caused by the lower energy position of the second peak in μ, which also shifts its spin-difference spectrum to lower energy.

Thus the only important discrepancy between theory (ρ_p) and experiment (μ) is the shift of the second peak in μ to lower energy. This is a general phenomenon, which occurs at a series of 1*s* x-ray-absorption spectra compared to ρ_p.[4,24] It can be related to the neglect of the core hole potential. For 3*d* silicides the effect of the core hole has been studied in detail by performing self-consistent supercell calculations.[24,25] It turned out that for these systems, and in general for all systems with relatively broad bands, the effects of the core hole can be described by the deformation of the density of states in which weight is shifted to lower energy. At the bottom of the respective bands intensity piles up; for details see Refs. 4, 26 and references therein. For the present study this implies that one expects the density of states to be deformed and intensity transferred to the Fermi level for the first peak and to the bottom of the band at +6.5 eV for the second peak. This is exactly what is observed and we conclude that the core hole effect explains the shift of the second peak to lower energy.

E. Determination of the Fano factor

The final point we want to discuss is the determination of the energy dependence of the Fano factor by making

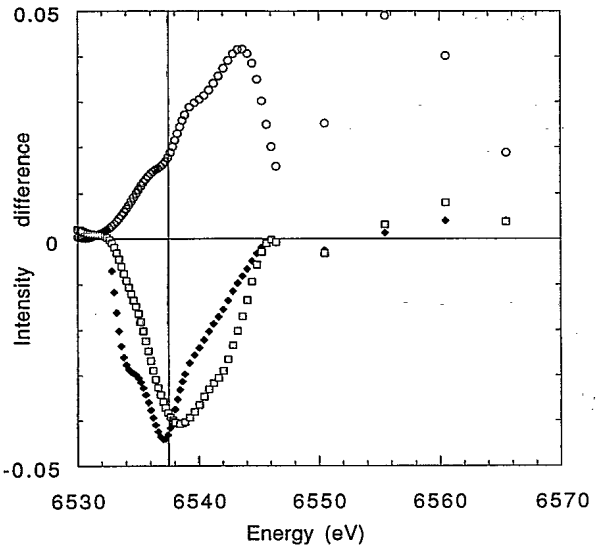

FIG. 5. Broadened (see text) local-spin-selective x-ray-absorption difference spectrum (open circles) compared with the broadened x-ray MCD spectrum multiplied with 50 (open squares). Their ratio is the Fano factor (solid diamonds), reaching −4% at the edge (vertical line). Above 6546 eV the 5 eV average values are given.

use of the division of the x-ray MCD spectrum by the local-spin-selective x-ray-absorption spectrum [Eq. (6)]. We have broadened both experimental spectra given in Fig. 3 with an additional Gaussian of 1.0 eV FWHM, in order to compare the results which were obtained with different experimental resolution.

Figure 5 compares both spectra obtained as such. The local-spin-selective x-ray-absorption spectrum (open circles) reaches +4%. The x-ray MCD spectrum (open squares) is multiplied with 50 in order to be visible on the same scale. It has a minimum of −4% in the plot which relates to $-4/50 = -0.08\%$. Only the energy range from 6520 eV to 6546 eV is given with individual points. Above 6546 eV the average value is given for the 5 eV energy ranges because otherwise the statistics of the present experiment is insufficient. Also if the value of the local-spin-selective x-ray-absorption spectrum is close to zero the determination of the Fano factor diverges; i.e., the statistical error becomes large. It can be seen that the Fano factor reaches its heighest value (−4%) at the edge, indicated with the thin vertical line. Its position is taken from the position of the Fermi level in Fig. 4. It decreases to a value lower than 1% above 7 eV. We conclude that in the energy range of the $3d$ band the matrix elements coupling the p states to the $1s$ core state are strongly affected. Due to the strong spin polarization of the $3d$ states combined with the essential $4p$ spin-orbit coupling the matrix elements for $p_{3/2}$ and $p_{1/2}$ are affected differently.

IV. CONCLUDING REMARKS

We have shown that one can use the $K\beta$ x-ray-emission channel to detect the local-spin-selective x-ray-absorption spectra. The analysis of the $K\beta$ spectral shape showed that one can detect spin-up and spin-down x-ray-absorption spectra seperately though with different resolution. Also the spin-up spectrum is affected by resonant Raman effects which can be taken out.

The local-spin-selective x-ray-absorption spectra are in accordance with the spin-polarized density of states as obtained from LMTO-ASA band-structure calculations. The comparison with x-ray MCD showed in both cases a large effect at the edge. It has been shown that by dividing the x-ray MCD spectrum by the local-spin-selective spectrum one is able to determine the Fano factor, including its energy dependence. For MnP it is found that the Fano factor reaches −4% at the edge and decreases to lower values above 7 eV. Clearly the Fano factor is shown to be strongly energy dependent. We note that even for MnP, which is not a favorable case, it turned out to be possible to obtain a reliable picture of the energy dependence of the Fano factor. Ferromagnetic systems with large moments, and for all systems containing divalent manganese, are expected to be measurable with considerably better statistics as well as with higher resolution because the spin-up spectrum can be measured for a single $3p$ state. Research is in progress to verify this.

The improved resolution obtained at the main peak of the $K\beta$ x-ray-emission spectrum promises to reveal many new details of the electronic structure of solids. The high-resolution structures at the edge reveal the quadrupolar transitions.[12] Also they are expected to reveal the existance of correlation effects beyond the used single-particle models in strongly correlated materials. A field which will be helped with high-resolution data is the interpretation of the pre-edge structures in iron compounds, for which a number of different models have been suggested.[27–29] The new $1s$ lifetime-free x-ray-absorption spectra have the promise to largely advance our understanding on this matter.

ACKNOWLEDGMENTS

We would like to thank Francois Baudelet and Lonny Berman for discussions and assistance during the experiments. We are grateful to D. Fruchart and J. Baruchel for the use of the MnP single crystals. F.d.G. would like to thank Ove Jepsen for his support for the LMTO calculations. This work was supported by the European Union program "Human Capital and Mobility," U.S. Department of Energy under Contract No. DE-AC02-76CH00016, and the Finnish Academy.

[1] K. Hämäläinen, C.C. Kao, J.B. Hastings, D.P. Siddons, L.E. Berman, V. Stojanoff, and S.P. Cramer, Phys. Rev. B **46**, 14 274 (1992).

[2] G. Peng, F.M.F. de Groot, K. Hämäläinen, J.A. Moore, X. Wang, M.M. Grush, J.B. Hastings, D.P. Siddons, W.H. Armstrong, O.C. Mullins, and S.P. Cramer, J. Am. Chem. Soc. **116**, 2914 (1994).

[3] B. Hermsmeier, C.S. Fadley, M.O. Krause, J. Jimenez-

Mier, P. Gerard, and S.T. Manson, Phys. Rev. Lett. **61**, 2592 (1988).
[4] F.M.F. de Groot, J. Electron. Spectrosc. **67**, 529 (1994).
[5] The density of states in presence of the core hole must be used, following the final state rule as given in U. von Barth and G. Grossmann, Phys. Rev. B **25**, 5150 (1982).
[6] G. Schütz, W. Wagner, W. Wilhelm, P. Kienle, R. Zeller, R. Frahm, and G. Materlik, Phys. Rev. Lett. **58**, 737 (1987).
[7] U. Fano, Phys. Rev. **178**, 131 (1969).
[8] B.N. Harmon and A.J. Freeman, Phys. Rev. B **10**, 1979 (1974).
[9] A. Mori, Y. Kayanuma, M. Nakazawa, and A. Kotani, J. Phys. Soc. Jpn. **63**, 306 (1994); A. Mori, Y. Kayanuma, and A. Kotani, Prog. Theor. Phys. **106**, 75 (1991).
[10] T. Aberg and B. Crasemann, in *X-ray Anomalous (Resonance) Scattering: Theory and Experiment*, edited by K. Fisher, G. Materlik, and C. Sparks (Elsevier, Amsterdam, 1994).
[11] L.E. Berman, J.B. Hastings, T. Oversluizen, and M. Woodle, Rev. Sci. Instrum. **63**, 428 (1992).
[12] K. Hämäläinen, D.P. Siddons, J.B. Hastings, and L.E. Berman, Phys. Rev. Lett. **67**, 2850 (1991).
[13] V. Stojanoff, K. Hämäläinen, D.P. Siddons, J.B. Hastings, L.E. Berman, S.P. Cramer, and G. Smith, Rev. Sci. Instrum. **63**, 1125 (1992).
[14] H. Tolentino, F. Baudelet, E. Dartyge, A. Fontaine, A. Lena, and G. Tourillon, Nucl. Instrum. Methods A **289**, 307 (1990).
[15] F. Baudelet, E. Dartyge, A. Fontaine, C. Brouder, G. Krill, J.P. Kappler, and M. Piecuch, Phys. Rev. B **43**, 5857 (1991).
[16] T. Komatsubara, T. Suzuki, and E. Hirahara, J. Phys. Soc. Jpn. **28**, 317 (1970).
[17] F.M.F. de Groot, A. Fontaine, C.C. Kao, and M. Krisch, J. Phys. Condens. Matter **6**, 6875 (1994).
[18] P. Eisenberger, P.M. Platzman, and H. Winick, Phys. Rev. B **13**, 2377 (1976).
[19] K. Hämäläinen, S. Manninen, P. Suortti, S.P. Collins, M.J. Cooper, and D. Laundy, J. Phys. Condens. Matter **1**, 5955 (1989).
[20] O.K. Andersen, Phys. Rev. B **12**, 3060 (1975).
[21] O.K. Andersen, O. Jepsen, and M. Sob, in *Electronic Band Structure and its Applications*, edited by M. Yussouff, Springer Lecture Notes (Springer, New York, 1987).
[22] S. Rundqvist, Acta Chem. Scand. **16**, 287 (1962).
[23] F.M.F. de Groot, O. Jepsen, and O.K. Andersen (unpublished).
[24] P.J.W. Weijs, M.T. Czyżyk, J.F. van Acker, W. Speier, J.B. Goedkoop, H. van Leuken, H.J.M. Hendrix, R.A. de Groot, G. van der Laan, K.H.J. Buschow, G. Wiech, and J.C. Fuggle, Phys. Rev. B **41**, 11 899 (1990).
[25] M.T. Czyżyk and R.A. de Groot, in *Proceedings of the 2nd European Conference on Progress in X-ray Synchrotron Radiation Research*, Rome, 1989, edited by A. Balerna, E. Bernieri, and S. Mobilio (Società Italiana di Fisica, Bologna, 1990), p. 47.
[26] J.F. van Acker, Ph.D. thesis, University of Nijmegen, 1990.
[27] S. Shadle, J. Penner-Hahn, H.J. Schugar, B. Hedman, K.O. Hodgson, and E.I. Solomon, J. Am. Chem. Soc. **115**, 767 (1993).
[28] B. Hannoyer, M. Lenglet, J. Dürr, and R. Cortes, J. Non-Cryst. Solids **151**, 209 (1992).
[29] G. Calas and J. Petiau, Solid State Commun. **45**, 625 (1983).